Joint Reconstruction of Activity and Attenuation in Time-of-Flight PET: A Quantitative Analysis

Ahmadreza Rezaei[1] (corresponding author), Christophe M Deroose[1], Thomas Vahle[2], Fernando Boada[3], Johan Nuyts[1]

[1] Nuclear Medicine and Molecular Imaging, KU Leuven, Leuven, Belgium.
[2] Siemens Healthcare GmbH, Erlangen, Germany.
[3] New York University Medical Center, New York, New York, USA.

CORRESPONDENCE:

Ahmadreza Rezaei, Department of Nuclear Medicine and Molecular Imaging, KU Leuven, Herestraat 49 - box 7003, 3000 Leuven, Belgium. Phone: +32 (163) 49080, Fax: +32 (163) 43759, Email: ahmadreza.rezaei@uz.kuleuven.be

FINANCIAL SUPPORT:

This work was supported in part by the Research Foundation Flanders (FWO) project G.0275.14N, FWO postdoctoral project 12T7118N and by the Center for Advanced Imaging Innovation and Research, a National Institute for Biomedical Imaging and Bioengineering Biomedical Technology Resource Center (NIH P41 EB017183).

SHORT TITLE:

Joint reconstruction in TOF-PET

KEYWORDS:

Quantitative Analysis, Joint reconstruction, Time-of-Flight PET

WORD COUNT:

5247

ABSTRACT

Joint activity and attenuation reconstruction methods from time of flight (TOF) positron emission tomography (PET) data provide an effective solution to attenuation correction when no (or incomplete/inaccurate) information on the attenuation is available. One of the main barriers limiting their use in clinical practice is the lack of validation of these methods on a relatively large patient database. In this contribution, we aim at validating the activity reconstructions of the maximum likelihood activity reconstruction and attenuation registration (MLRR) algorithm on a whole-body patient data set. Furthermore, a partial validation (since the scale problem of the algorithm is avoided for now) of the maximum likelihood activity and attenuation reconstruction (MLAA) algorithm is also provided. We present a quantitative comparison of the joint reconstructions to the current clinical gold-standard maximum likelihood expectation maximization (MLEM) reconstruction with computed tomography (CT) based attenuation correction. **Methods:** The whole-body TOF-PET emission data of each patient data set is processed as a whole to reconstruct an activity volume covering all the acquired bed positions, which helps to reduce the problem of a scale per bed position in MLAA to a global scale for the entire activity volume. Three reconstruction algorithms are used: MLEM, MLRR and MLAA. A maximum likelihood (ML) scaling of the single scatter simulation estimate to the emission data is used for scatter correction. The reconstruction results are then analyzed in different regions of interest. **Results:** The joint reconstructions of the whole-body patient data set provide better quantification in case of PET and CT misalignments caused by patient and organ motion. Our quantitative analysis shows a difference of - 4.2% (±2.3%) and -7.5% (±4.6%) between the joint reconstructions of MLRR and MLAA compared to MLEM, averaged over all regions of interest, respectively. **Conclusion:** Joint activity and attenuation estimation methods provide a useful means to estimate the tracer distribution in cases where CT-based attenuation images are subject to misalignments or are not available. With an accurate estimate of the scatter contribution in the emission measurements, the joint TOF-PET reconstructions are within clinical acceptable accuracy.

INTRODUCTION

Since it was shown that time of flight (TOF) positron emission tomography (PET) data provide information about the attenuating medium of the emission data (*1*), a number of algorithms have been developed to exploit the added information available with TOF. The majority of the newly developed methods aim at simultaneously reconstructing an activity and an attenuation image from the TOF-PET emission data (*2*–*4*). Furthermore, several methods have been proposed which avoid the reconstruction of the attenuation medium and attempt to estimate the attenuation correction values which more directly influence the TOF emission measurements (*5*–*7*). However, in event-based reconstructions methods which avoid the histogramming of emission data (e.g. origin ensembles, listmode reconstructions algorithms etc.), the attenuation correction values can no longer be estimated, but instead their back-projection (also commonly referred to as the “sensitivity image”) can (*8*,*9*).

It is known that the attenuation information available by TOF emission data does not allow a quantitative assessment of the reconstructed distribution of activity, as TOF-PET data determine the activity distribution only up to a constant scale. This limiting factor might be the main reason why joint estimation methods have not yet been introduced and used in clinical practice. Recently, methods have been proposed that take advantage of available computed tomography (CT) images of the patient (*10*–*12*), which are commonly available in state-of-the-art TOF-PET/CT scanners. Where the method introduced in (*10*) aims at completing the sinogram of the attenuation correction factors for planes for which no CT measurements are available, the methods introduced in (*11*,*12*) aim at deforming the CT-based attenuation image to correct for any possible mismatch between the CT and PET acquisitions. As a result of using the energy-adjusted CT images in the joint reconstruction framework, the scale problem is automatically overcome. Apart from these methods which use the added information of the CT, other scale correction techniques for joint activity and attenuation reconstructions exist in the literature which include: methods which use tissue prior maps for a more optimal initialization of the joint reconstruction algorithm (*13*) or for utilizing an intensity prior during reconstruction on expected tissue values being reconstructed (*4*,*14*), methods which attempt to solve the problem by adding transmission

sources in the scanner (*15*,*16*) or by using the lutetium background radiation source as the transmission source (*17*), and methods which ambitiously try to determine the scale from the scattered events in the emission data (*18*).

Other limiting factors for the use of joint reconstruction methods in clinical practice are the diagnostic value of the CT images and the lack of a comprehensive validation of these methods on a big patient database. Although studies have been performed on a number of patient data sets, the studies have been mainly restricted to 3D simulations often times even ignoring some of the data corrections routinely done in clinical practice (e.g. scatter/randoms corrections). An initial study was done in (19) where after taking the scale problem into account, the results of the joint estimation method were found to be similar to the gold-standard without the effects of motion. It was found in (20–22) that the joint reconstruction results outperform methods which utilize an magnetic resonance (MR) based attenuation correction scheme for attenuation correction of the TOF-PET emission data. The studies demonstrate that the joint reconstruction methods were able to remove MR-related artifacts which otherwise propagate into the emission reconstruction. In (23), the joint estimation methods were analyzed in a retrospective cardiac study on a relatively bigger patient dataset. As expected it was found that the joint reconstruction method proposed was able to remove the possible PET/CT mismatch and furthermore demonstrate the influence of a CT mismatch. The study also demonstrated that the CT-mismatch affects the scatter estimate, which in turn has an effect on the final reconstruction. However in a more recent study (24), the joint reconstruction method was found to give more bias in the reconstructed activity images compared to results obtained with an atlas-based correction of attenuation in a collection of 18F-FDG brain scans. The accuracy of the MLACF joint estimation method was also analyzed on a population of patient brain scans (25). The authors report that the joint estimation images were comparable to the gold-standard MLEM reconstructions with CT-based attenuation correction once a plane-dependent scaling of the activity was applied.

In this study we perform a quantitative analysis of activity images from two joint reconstruction algorithms, comparing them to the current clinical gold-standard (i.e. MLEM with a CT-based attenuation correction of the emission data), on a set of whole-body patient scans. The paper is organized as follows. In section 2 we describe the reconstruction and image analysis parameters. The results are presented in section 3 and discussed in section 4.

MATERIALS AND METHODS

Data Acquisition and Processing

A total of 23 whole-body ^{18}F-FDG patient scans were acquired on the Siemens Biograph mCT scanner (26) at the New York University Medical Center. The local institutional review board approved this study and informed consent was obtained from all subjects. On average each patient was injected with 550 MBq of the ^{18}F-FDG tracer and scanned an hour post-injection. The emission data were acquired in 5-8 different bed positions, each scanned for 120 s per bed position. The data were collected in 5D sinograms consisting of 400 radial bins of 2.005 mm width, 168 azimuth angles over 180 degrees, a combined 621 planes of 2.027 mm width for the direct and oblique (segments ±1, ±2, …) planes and 13 TOF-bins of 312 ps width. The e7tools provided by Siemens were used to process the raw data and to generate the expected scatter and randoms contribution of the emission measurements independently for each bed position. Since the joint estimation methods estimate more parameters than the standard MLEM algorithm, they tend to respond differently to data inconsistencies (see supplementary material of (27)). This can lead to an underestimation of the joint estimation performance compared to the gold standard MLEM. Hence, as proposed in (27), a plane-dependent maximum likelihood (ML) scaling of the single scatter simulation (28) estimate was estimated from the emission data. This maximum likelihood scaling of the single scatter simulation estimate was used for scatter correction during reconstructions.

Reconstructions

The entire scanned part of the patient body was reconstructed in a single volume, using the TOF-PET emission data from all bed positions simultaneously. The in-house projector still worked on a bed-

by-bed basis but the (back/) projections were computed (onto) from a single whole-body volume. Prior to reconstruction, the data were mashed in the radial direction with a mashing factor of 2, and the activity and attenuation images were consequently reconstructed in a 200 × 200 pixel grid of 4.0724 mm width transaxially and up to 543 planes of 2.007 mm width axially. The TOF resolution of the scanner was modelled as a Gaussian which after convolution with a top-hat binning window of 312 ps gives an effective resolution of 580 ps full width at half maximum. In this study, three algorithms were used to reconstruct the tracer distribution uptake;

1. maximum likelihood expectation maximization (MLEM) which makes use of the available CT-based attenuation correction values,
2. maximum likelihood activity reconstruction and attenuation registration (MLRR) (*11*) which aims to reconstruct an activity image while deforming an available CT-based attenuation image such that the pair of images best fit the measurements, and
3. maximum likelihood activity and attenuation (MLAA) (*3*) which reconstructs an activity image together with an attenuation image directly from the emission data.

The MLEM reconstructions are obtained after 3 iterations and 24 subsets. The MLRR reconstructions are obtained with the same iteration scheme, and in each of these 72 sub-iterations the activity was updated once and the attenuation three times. A uniform activity image inside the field of view is used to initialize the algorithm together with the zero vector displacement field. The displacement field is only updated inside the patient support, computed from the CT-based attenuation image, and is regularized by a fluid-like and diffusion-like regularization of the displacement field.

In the case of MLAA, the activity and attenuation reconstructions are obtained after 5 iterations of 24 subsets where the attenuation image was updated three times for each update of the activity reconstruction. The algorithm was initialized with uniform activity in the field of view and uniform tissue attenuation (0.095 cm^{-1}) in the patient support. In order to eliminate any confounding effects of the scale factor in the reconstructions, the scale problem in MLAA was fixed by imposing the total tracer activity of the MLEM reconstruction. The total tracer activity of MLEM was computed within a volume inside the patient support, excluding regions that could be affected by patient/respiratory motion, e.g. lungs and their neighboring regions and exactly the same volume was used to scale the MLAA image during iterations. A thresholding of the CT-based attenuation image was used to extract patient lungs, which was followed by a morphological dilation (with an elliptical neighborhood kernel of 2 cm and 3 cm radius in the transaxial and axial directions) of the mask to limit the influence of motion-affected regions.

Because the convergence of MLRR, MLAA and MLEM may be different, “standard” activity images are produced by standard MLEM reconstructions (3 iterations of 24 subsets) using the MLRR and MLAA attenuation estimates. In the following we will refer to these images as MLAA or MLRR activity reconstructions, although they actually are MLEM reconstructions obtained with the MLAA or MLRR attenuation maps. In all cases the final activity reconstruction was post-smoothed with a Gaussian of 6 mm full width at half maximum.

Image Analysis

The activity reconstructions are compared and evaluated in different regions of interest (ROIs). A separate mask is generated by segmenting the bladder, liver, heart, a lumbar vertebra and some tumor/inflammatory lesions with high local tracer uptake. These organ masks were generated by thresholding the MLAA reconstructed activity image. The CT-based attenuation image was also used for the segmentation of the spinal region, which provided an initial mask for the delineation of the lumbar vertebrae. The bladder and the lumbar vertebra regions were chosen to report on the behavior of the algorithms in regions where no patient motion was expected. The liver region was chosen as its activity is typically used as reference, and the dome of the liver occasionally suffers from attenuation correction errors due to breathing induced mismatches between PET and CT. The heart region as well as the tumor/inflammatory lesions are the clinically relevant regions in patient studies, which are typically subject to in-scan patient motion.

In our comparative analysis, the mean difference between two activity reconstructions, X and Y, being compared was computed in all the segmented regions of interest as:

$$diff(X,Y) = \frac{\sum_{j\in ROI} Y_j - \sum_{j\in ROI} X_j}{\sum_{j\in ROI} X_j} \qquad (1)$$

where *X* is considered the reference method. The mean and, in brackets, the standard deviation are reported throughout the text. When combining differences of multiple regions/patients, the mean and standard deviations are reported for the absolute value of region/patient differences.

RESULTS

Figures 1 and 2 show the mean differences observed between MLRR and MLAA activity reconstructions compared to the ground truth MLEM reconstruction for the segmented bladder and vertebrae regions, respectively. On average, the MLRR and MLAA reconstructions resulted in a relative difference of -3.6% (±1.7%) and -8.1% (±7.0%) for the bladder region, respectively. In the segmented vertebrae region, the average difference between the reconstructions were -2.4% (±1.8%) and -8.7% (±4.4%) for the MLRR and MLAA activity reconstructions, respectively.

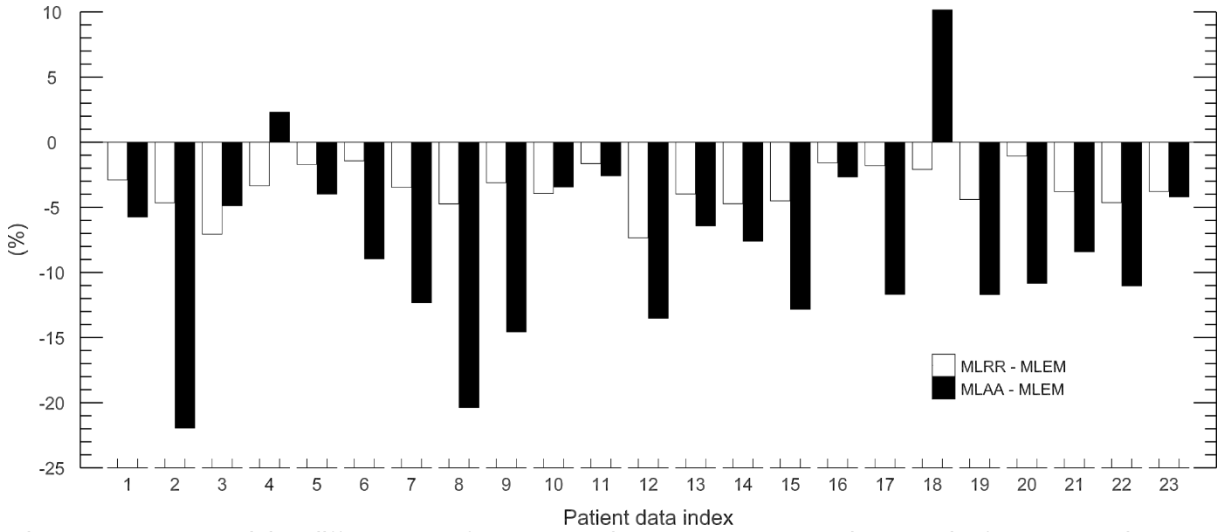

Figure 1: *Mean activity differences of MLRR and MLEM reconstructions and of MLAA and MLEM reconstructions in the bladder region. The bladder to liver ratios of our patient database is given in supplemental figure 1.*

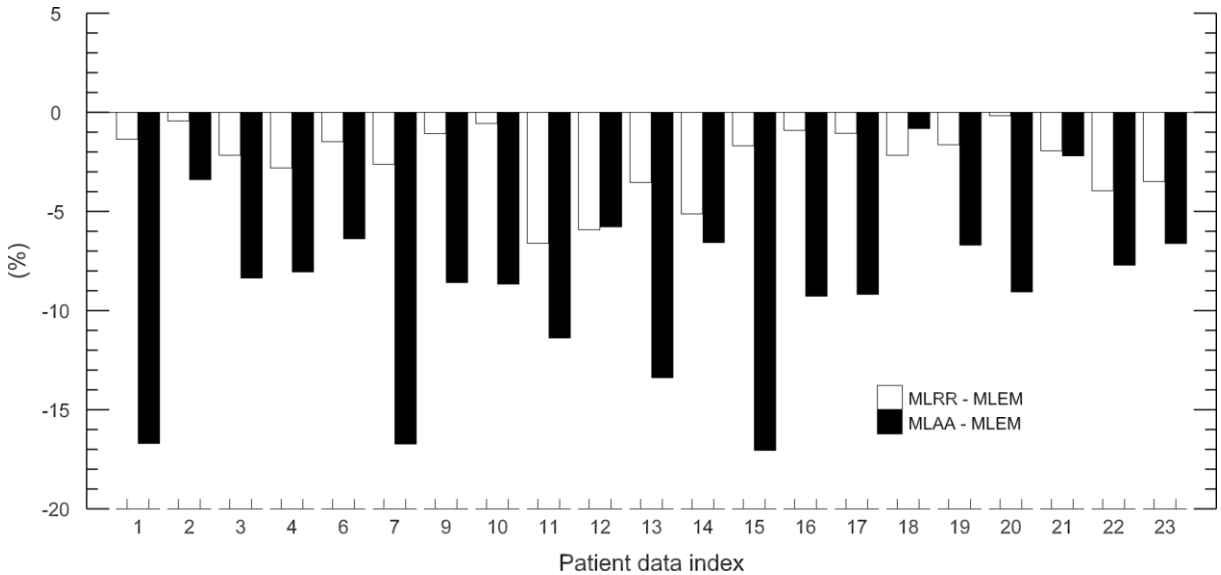

Figure 2: *Mean activity differences of MLRR and MLEM reconstructions and of MLAA and MLEM reconstructions in the segmented vertebrae region. The vertebrae to liver ratios of our patient database is given in supplemental figure 1.*

In the hope to get more insight into the differences observed in MLAA, a new set of MLAA activity images were reconstructed. This time the MLAA attenuation image was initialized with the deformed

CT-based attenuation image of MLRR and the MLAA activity image with the corresponding MLEM activity image (i.e. MLEM of 3 iterations and 24 subsets using the deformed CT-based attenuation image). The mean differences of these MLAA reconstructions with the ground truth MLEM and with the original MLAA images was -8.5% (±7.0%) and -0.1% (±1.1%) for the bladder region, respectively. Similar results were obtained for the vertebrae region with a difference of -7.6% (±5.4%) and 1.3% (±1.1%), respectively. Furthermore, the likelihood was computed by forward projection of the reconstructions obtained with the CT-based, MLRR-based and MLAA-based attenuation images. We found the likelihood of MLAA to be on average 2.7% higher than that of MLRR, which in turn was 4.2% higher than that of MLEM. This suggests that the observed differences are not related to the convergence of MLAA reconstructions. We have reason to believe that this increase of the likelihood is due to inconsistencies present in the data due to e.g. the attenuation image, scanner calibrations, etc. which are better accounted for in MLAA than in MLRR and better in MLRR than in MLEM. The segmented bladder to liver contrast as well as the average contrast of the segmented vertebral region to the liver can be found in the supplementary material.

In standard practice a volume of interest well within the liver region is segmented to quantify the activity concentration in the liver. However, the CT data are often acquired and reconstructed in a breathing phase that differs from the average breathing pose of the PET scan, which could result in significant artifacts in the activity reconstructions of the PET emission data. Figure 3 shows such a case where the CT and PET data are acquired at two different phases of the breathing cycle. Whereas the MLEM reconstruction is greatly affected by the between-scan mismatch, the MLAA reconstruction is able to provide accurate values in the motion-affected area. In spite of such extensive internal motion, the MLRR reconstruction was also able to produce a motion corrected reconstruction using a deformed CT attenuation image.

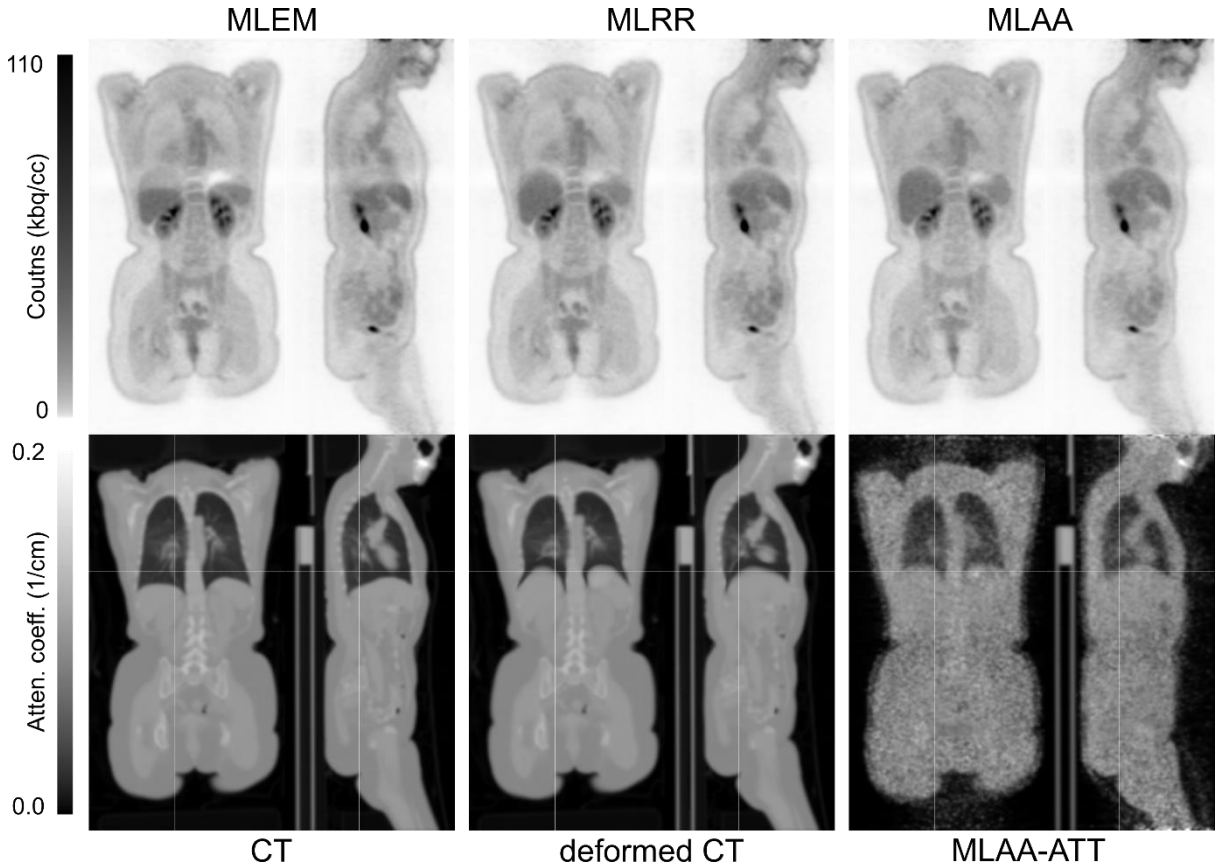

Figure 3: *Activity (top) and attenuation (bottom) reconstructions of MLEM (left), MLRR (center) and MLAA (right) for a patient dataset where the CT (bottom-left) and PET data were acquired at different phases of the breathing cycle.*

An initial naive segmentation of the liver region (which included most of the liver and therefore possible motion affected areas) was used to compare the reconstruction results. The subsequent comparison of the activity reconstructions resulted in a difference of 2.0% (±18.5%) and 0.4% (±32.0%)

between the MLRR and MLAA reconstructions compared to the reference MLEM activity reconstruction, respectively. Further improving the segmented liver region by avoiding the superior parts of the liver that could be affected by motion, an average difference of -2.8% (±2.1%) was computed for the MLRR and MLEM reconstructions over all our patient database. For the MLAA algorithm, the average difference was -7.9% (±5.9%). A bar plot of the quantification results of the segmented liver region is shown in figure 4.

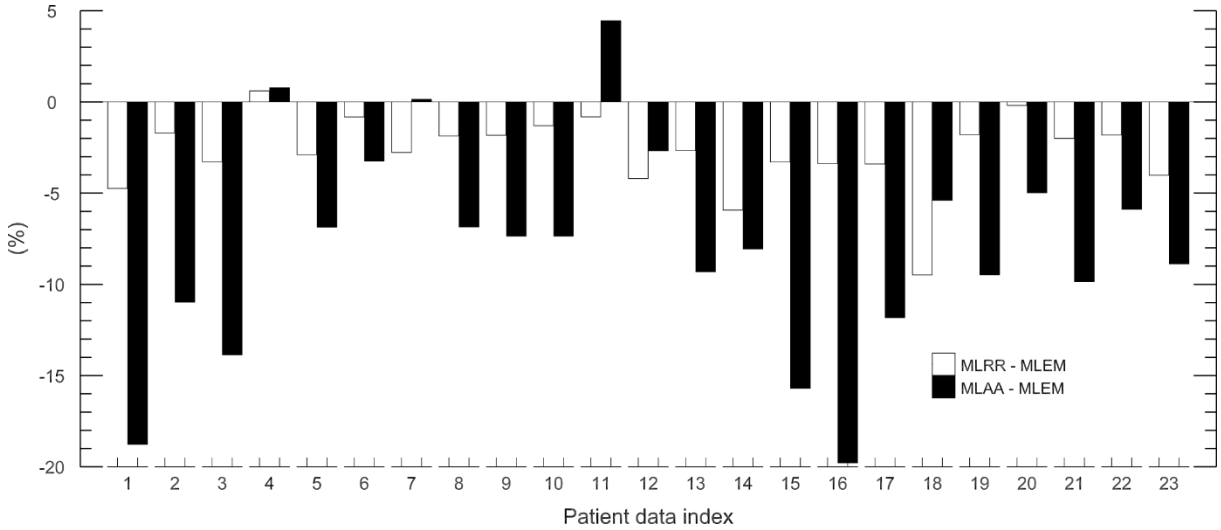

Figure 4: *Mean activity differences of MLRR and MLEM reconstructions and of MLAA and MLEM reconstructions in the segmented liver region (avoiding the superior parts of the liver which are expected to be affected by motion).*

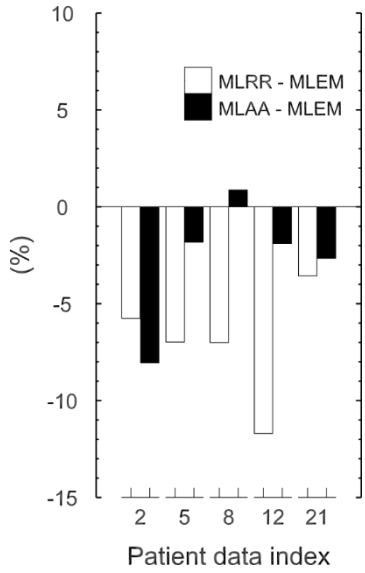

Figure 5: *Mean activity differences of MLRR/MLAA and MLEM reconstructions in the heart region.*

Figure 5 shows the results on the relative differences of the MLRR/MLAA and the reference MLEM activity reconstructions in the segmented heart region for 5 (22%) patient reconstructions with myocardial ^{18}F-FDG uptake. Comparison of the joint reconstructions of MLRR and MLAA to the reference MLEM activity reconstruction resulted in an average relative difference of -7.0% (±3.1%) and -2.7% (±3.3%), respectively.

A total of 58 lesions with a high local activity uptake were segmented which included tumors of different organs and inflammatory lesions with abnormal high activity. It should be noted that only 15 of the 23 patient scans (65%) were used in this study, as there were no such lesions found in the other 8 whole body images. Also, a maximum number of 5 lesions were selected for each patient. Whenever possible lesions were selected from different organs and larger lesions were selected to avoid problems related to partial volume effect. The average difference between MLRR/MLAA and MLEM activity

reconstructions were -5.3% (±3.2%) and -7.9% (±5.4%), respectively. The quantification results of the tumor/inflammatory lesions is shown in figure 6 and a histogram of the ratio of these high activity lesions to the liver activity can be found in the supplementary material.

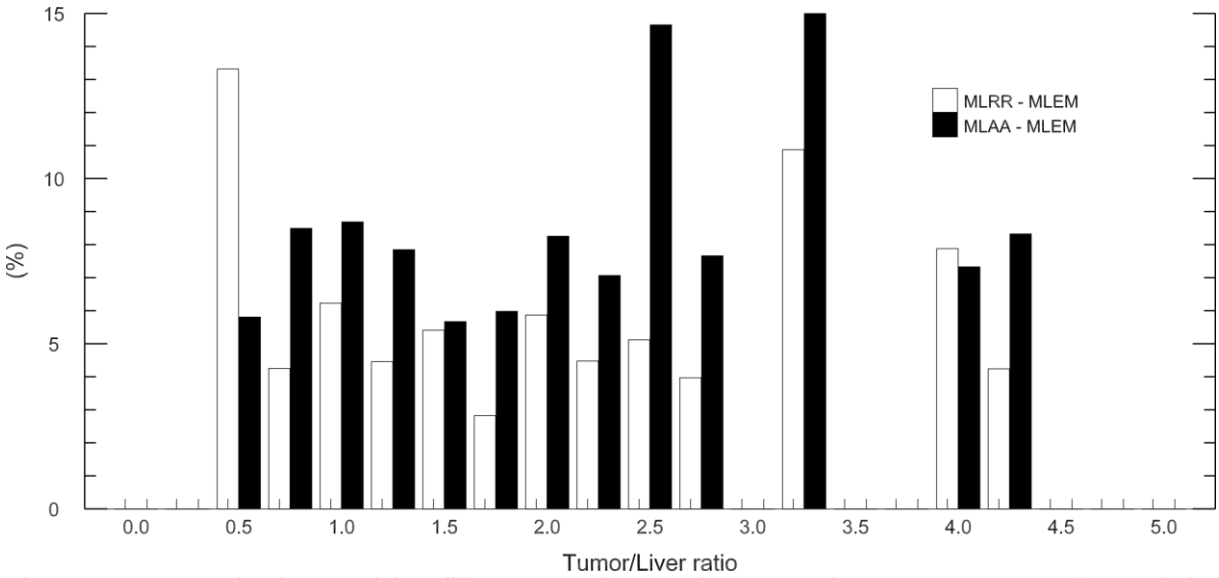

Figure 6: *Mean absolute activity differences of MLRR/MLAA and MLEM reconstructions of the segmented high local activity uptake lesions. A histogram of the high activity lesions classified based on their tumor to liver ratios is provided in the supplemental figure 2.*

The segmented lesions were manually classified based on their location into lesions which could potentially be affected by motion and lesions which were less likely to be affected by motion. Lesions located in the mediastinum and the ones within or in close proximity of the lungs were regarded as motion-affected lesion. Table 1 reports the results for these two clusters of lesions as well as the overall differences in all the segmented regions.

Table 1: *ROI differences between MLRR/MLAA and the reference MLEM activity reconstructions for the tumor/inflammatory lesions with high local tracer uptake.*

	MLRR – MLEM (%)	MLAA – MLEM (%)
all (58)	-5.3 (± 3.2)	-7.9 (± 5.4)
non motion-affected (35)	-4.4 (± 2.9)	-9.3 (± 6.0)
motion-affected (23)	-6.6 (± 3.3)	-5.7 (± 3.4)

DISCUSSION

In this study we have tried to validate the joint reconstructions of MLRR and MLAA to the current clinical gold-standard which is the activity reconstruction of MLEM with a correction of the attenuation using a CT attenuation image adjusted to the 511 keV photon energy of PET. To insure a comparison of the reconstructions at a similar convergence level, “standard” activity images were generated following the attenuation estimation of the joint reconstruction methods. Although a slightly different noise structure was observed between the final MLAA activity reconstruction and the “standard” activity reconstructions, the differences were minimal in ROI-based quantifications. Therefore, in clinical practice this additional reconstruction would not be necessary. We observe that in case of a CT and PET mismatch the attenuation values that are computed from the adjusted CT image could directly (and also possibly indirectly through the scatter shape) influence the quantification results.

In the bladder and lumbar vertebrae results (regions not expected to be affected by motion), the MLRR reconstructions were quantitatively comparable to the gold-standard MLEM reconstructions. However, some discrepancies were observed when comparing MLAA tracer activity distributions. Hence, MLAA reconstructions were repeated with MLRR-based initialization to verify if differences

between MLAA and MLEM/MLRR could be due to convergence differences between the algorithms. We found that MLAA iterates away from the initial MLRR-based attenuation images, and in all cases achieves a higher likelihood. We believe this to be a fundamental issue, since it shows that MLAA manages to find a solution that better explains the data (higher likelihood) that is outside the solution set available to MLEM and MLRR. We previously reported that in case of inconsistencies in data corrections, MLAA and MLEM converge to different solutions (*27*). Hence, the differences observed between the reconstructions can hint to residual data inconsistencies which make them converge to slightly different solutions.

The results on the liver region show that MLRR and MLAA produce a very different attenuation correction near the dome of the liver, which based on visual analysis, was attributed to mismatches due to respiratory motion. When only the lower part of the liver was compared, a much better agreement between all algorithms was observed, as expected since the attenuation of the lower part of the liver is much less affected by respiration. In an attempt to quantify the indirect influence of the PET and CT mismatch through the estimated shape of the scatter as reported in (*23*), all the reconstructions were repeated with the MLRR-based estimate of the scatter. However, we found that this had a marginal effect in our comparative analysis (results not shown here).

The MLRR and MLAA results on the segmented heart region were in slight contrast to other regions of interest analyzed in this study. We believe that parts of this discrepancy can be explained by the inconsistencies in the emission data due to in-scan respiratory and cardiac motion (29). Whereas MLAA is free to assign and adjust the attenuation values of motion affected regions, MLRR does not have this freedom and is only able to manipulate tissue boundaries. It is possible that this also explains the higher differences observed in MLRR between the motion affected and the non-motion affected inflammatory lesion of table 1.

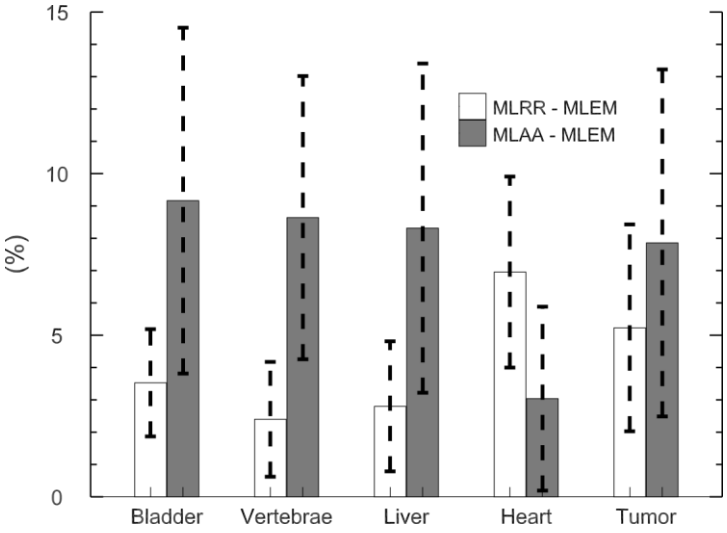

Figure 7: *Mean activity differences of MLRR/MLAA and MLEM reconstructions of all the ROIs analyzed in this study.*

In this study we have focused on quantifying the similarities and differences, in different regions of interest, between the joint reconstructions of MLRR/MLAA and the clinical gold-standard MLEM reconstruction. Figure 7 shows the average ROI-based differences observed between the reconstructions for all the different regions analyzed in the study. As mentioned earlier, to avoid problems related to the scale in MLAA, the total tracer activity of MLEM (in a reliable tissue region) was used to scale the MLAA activity reconstruction. In clinical practice, this would not be possible when no CT image is available. As briefly outlined in the introduction, several methods have been proposed to determine the scale factor (10–18). In a clinical setting, the most practical way of obtaining quantitative MLAA reconstructions would be to use a method which either limits or encourages (*4*) the reconstructed attenuation values to pre-defined tissue attenuation values. MLRR however, does not have the scale problem. In cases where the CT-based attenuation image is available, MLRR provides a better alternative than MLEM in regions expected to be affected by motion and is similar to the clinical gold-standard, otherwise. This is also to some extent reflected in figure 7 as higher differences are observed in the heart region which is subject to between-scan and in-scan motions. Compared to the results

shown for MLRR, the differemces between MLAA and MLEM activity images are larger. As mentioned above, we believe these differences are caused by data inconsistencies. These can be reduced by applying a more accurate calibration of the scanner (e.g. crystal/geometric sensitivities, TOF resolutions/offsets, etc.), and in ongoing work, we observe that doing so indeed reduces the differences between MLAA and MLEM activity reconstructions. Therefore, we postulate that the differences observed in our study are mostly due to residual inconsistencies caused by inaccuracies in the corrections applied during reconstruction.

CONCLUSION

In an attempt to validate the joint activity and attenuation reconstructions from TOF-PET emission data, reconstructions of whole body scans of a patient dataset were quantitatively analyzed and compared to the current clinical gold-standard. Our study demonstrates that in the presence of patient motion and provided that an accurate estimate of the scatter is available, the joint activity and attenuation reconstructions from TOF-PET provide a more accurate reconstruction of the tracer distribution compared to the current gold-standard. In regions not affected by motion, the differences between MLRR and MLEM were small (typically below 5%). The differences between MLAA and MLEM were larger, exceeding 10% in several cases. We believe that these differences are at least partly caused by data inconsistencies, and it is therefore not yet clear which of these reconstructions is the more accurate one. The problem of obtaining an accurate scale for the joint reconstruction is eliminated in the case of MLRR where CT-based attenuation information is available.

ACKNOWLEDGMENTS

This work was supported in part by the Research Foundation Flanders (FWO) project G.0275.14N, FWO postdoctoral project 12T7118N and by the Center for Advanced Imaging Innovation and Research, a National Institute for Biomedical Imaging and Bioengineering Biomedical Technology Resource Center (NIH P41 EB017183).

REFERENCES

1. Defrise M, Rezaei A, Nuyts J. Time-of-flight PET data determine the attenuation sinogram up to a constant. *Phys Med Biol*. 2012;57:885–99.
2. Salomon A, Goedicke A, Schweizer B, Aach T, Schulz V. Simultaneous reconstruction of activity and attenuation for PET/MR. *IEEE Trans Med Imaging*. 2011;30:804–13.
3. Rezaei A, Defrise M, Bal G, et al. Simultaneous reconstruction of activity and attenuation in time-of-flight PET. *IEEE Trans Med Imaging*. 2012;31:2224–33.
4. Mehranian A, Zaidi H. Joint Estimation of Activity and Attenuation in Whole-Body TOF PET/MRI Using Constrained Gaussian Mixture Models. *IEEE Trans Med Imaging*. 2015;34:1808–1821.
5. Rezaei A, Defrise M, Nuyts J. ML-reconstruction for TOF-PET with simultaneous estimation of the attenuation factors. *IEEE Trans Med Imaging*. 2014;33:1563–72.
6. Li H, El Fakhri G, Li Q. Direct MAP Estimation of Attenuation Sinogram using TOF PET Data and Anatomical Information. In: 2013 Fully Three-Dimensional Image Reconstr. Radiol. Nucl. Med. Proc. Vol 3. ; 2013:405–408.
7. Salvo K, Defrise M. sMLACF: a generalized expectation-maximization algorithm for TOF-PET to reconstruct the activity and attenuation simultaneously. *Phys Med Biol*. 2017.
8. Rezaei A, Bickell M, Fulton R, Nuyts J. Joint Activity and Attenuation Reconstruction of Listmode TOF-PET data. In: 2015 IEEE Nucl. Sci. Symp. Med. Imaging Conf. (2015 NSS/MIC). ; 2015.
9. Herraiz JL, Sitek A. Sensitivity estimation in time-of-flight list-mode positron emission tomography. *Med Phys*. 2015;42:6690-6702.
10. Panin VY, Defrise M, Nuyts J, Rezaei A, Casey ME. Reconstruction of uniform sensitivity emission image with partially known axial attenuation information in PET-CT scanners. In: 2012 IEEE Nucl. Sci. Symp. Med. Imaging Conf. Rec. (2012 NSS/MIC). IEEE; 2012:2166–2173.

11. Rezaei A, Michel C, Casey ME, Nuyts J. Simultaneous reconstruction of the activity image and registration of the CT image in TOF-PET. *Phys Med Biol*. 2016;61:1852-1874.
12. Bousse A, Bertolli O, Atkinson D, et al. Maximum-Likelihood Joint Image Reconstruction/Motion Estimation in Attenuation-Corrected Respiratory Gated PET/CT using a Single Attenuation Map. *IEEE Trans Med Imaging*. 2015;35:1-1.
13. Cheng J-C (Kevin), Salomon A, Yaqub M, Boellaard R. Investigation of practical initial attenuation image estimates in TOF-MLAA reconstruction for PET/MR. *Med Phys*. 2016;43:4163-4173.
14. Ahn S, Cheng L, Shanbhag D, Wiesinger F, Manjeshwar R. Joint reconstruction of activity and attenuation using MR-based priors: Application to clinical TOF PET/MR. In: 2015 IEEE Nuclear Science Symposium and Medical Imaging Conference (NSS/MIC). ; 2015:1-4.
15. Panin VY, Aykac M, Casey ME. Simultaneous reconstruction of emission activity and attenuation coefficient distribution from TOF data, acquired with rotating external line source. In: 2011 IEEE Nucl. Sci. Symp. Conf. Rec. Vol 3649. IEEE; 2011:4329–4336.
16. Mollet P, Keereman V, Clementel E, Vandenberghe S. Simultaneous MR-compatible emission and transmission imaging for PET using time-of-flight information. *IEEE Trans Med Imaging*. 2012;31:1734–1742.
17. Rothfuss H, Panin V, Moor A, et al. LSO background radiation as a transmission source using time of flight. *Phys Med Biol*. 2014;59:5483-5500.
18. Berker Y, Kiessling F, Schulz V. Scattered PET data for attenuation-map reconstruction in PET/MRI. *Med Phys*. 2014;41:102502.
19. Hamill JJ, Panin VY. TOF-MLAA for attenuation correction in thoracic PET/CT. In: 2012 IEEE Nucl. Sci. Symp. Med. Imaging Conf. Rec. IEEE; 2012:4040–4047.
20. Boellaard R, Hofman MBM, Hoekstra OS, Lammertsma AA. Accurate PET/MR quantification using time of flight MLAA image reconstruction. *Mol Imaging Biol*. 2014;16:469–477.
21. Lougovski A, Schramm G, Maus J, Hofheinz F, van den Hoff J. Preliminary evaluation of the MLAA algorithm with the Philips Ingenuity PET/MR. *EJNMMI Phys*. 2014;1:A33.
22. Mehranian A, Zaidi H. Clinical Assessment of Emission- and Segmentation-Based MR-Guided Attenuation Correction in Whole-Body Time-of-Flight PET/MR Imaging. *J Nucl Med*. 2015;56:877-883.
23. Presotto L, Busnardo E, Perani D, Gianolli L, Gilardi MC, Bettinardi V. Simultaneous reconstruction of attenuation and activity in cardiac PET can remove CT misalignment artifacts. *J Nucl Cardiol*. 2015.
24. Mehranian A, Arabi H, Zaidi H. Quantitative analysis of MRI-guided attenuation correction techniques in time-of-flight brain PET/MRI. *NeuroImage*. 2016;130:123-133.
25. Bal H, Panin VY, Platsch G, et al. Evaluation of MLACF based calculated attenuation brain PET imaging for FDG patient studies. *Phys Med Biol*. 2017;62:2542.
26. Jakoby BW, Bercier Y, Conti M, Casey ME, Bendriem B, Townsend DW. Physical and clinical performance of the mCT time-of-flight PET/CT scanner. *Phys Med Biol*. 2011;56:2375–89.
27. Rezaei A, Salvo K, Vahle T, et al. Plane-dependent ML scatter scaling: 3D extension of the 2D simulated single scatter (SSS) estimate. *Phys Med Biol*. 2017;62:6515.
28. Watson CC. Extension of Single Scatter Simulation to Scatter Correction of Time-of-Flight PET. *IEEE Trans Nucl Sci*. 2007;54:1679-1686.
29. Rezaei A, Nuyts J, Defrise M. The Effect of Motion on Joint Estimates of Activity and Attenuation from Time-of-Flight PET Data. In: 2013 Fully Three-Dimensional Image Reconstr. Radiol. Nucl. Med. Proc. ; 2013:297-300.

Joint reconstruction of activity and attenuation in Time-of-Flight PET: A Quantitative Analysis

Ahmadreza Rezaei[1] (corresponding author), Christophe M Deroose[1], Thomas Vahle[2], Fernando Boada[3], Johan Nuyts[1]

[1] Nuclear Medicine and Molecular Imaging, KU Leuven, Leuven, Belgium.
[2] Siemens Healthcare GmbH, Erlangen, Germany.
[3] New York University Medical Center, New York, New York, USA.

SUPPLEMENTARY MATERIAL

To give an idea of the tracer uptake in the bladder and the vertebrae, supplemental figure 1 shows the bladder to liver and the vertebra to liver ratios for all patients in our patient database. These ratios were obtained from the reference MLEM reconstructions (CT-based attenuation correction). Supplemental figure 2 shows a histogram of the high activity lesions classified based on their tumor to liver ratios that were used to analyze differences between MLRR/MLAA and MLEM as shown in figure 6.

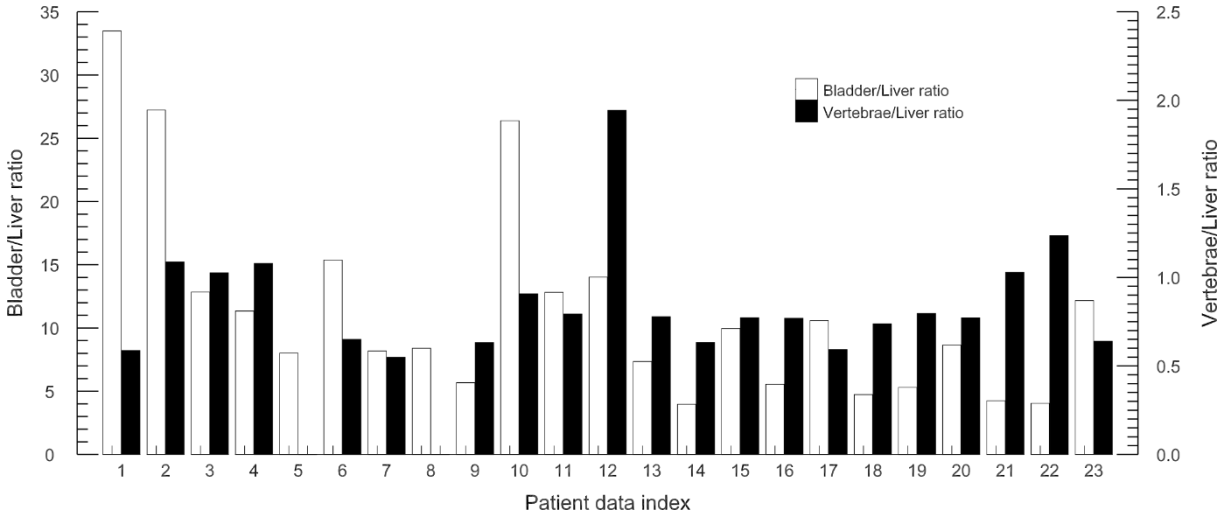

Supplemental Figure 1: *Bladder to liver and vertebra to liver ratios computed as the average activity inside the segmented bladder and vertebra regions to the average activity inside the liver.*

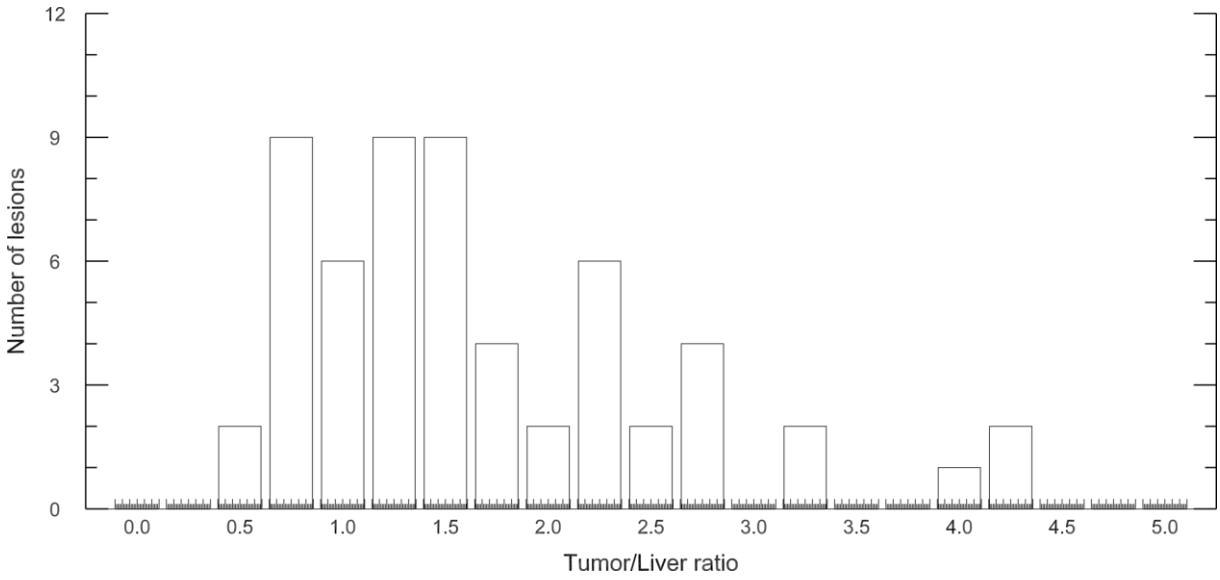

Supplemental Figure 2: *Histogram of the tumors classified by their tumor to liver ratio.*